Hindawi Publishing Corporation
Journal of Nanomaterials
Volume 2016, Article ID 9510156, 13 pages
http://dx.doi.org/10.1155/2016/9510156

Research Article

Extreme Wetting-Resistant Multiscale Nano-/Microstructured Surfaces for Viscoelastic Liquid Repellence

Aoythip Chunglok,[1,2] Nantakan Muensit,[1,2] and Chalongrat Daengngam[1,2]

[1]*Department of Physics, Faculty of Science, Prince of Songkla University, Songkhla 90110, Thailand*
[2]*Center of Excellence in Nanotechnology for Energy (CENE), Prince of Songkla University, Songkhla 90110, Thailand*

Correspondence should be addressed to Chalongrat Daengngam; chalongrat.d@psu.ac.th

Received 18 May 2016; Accepted 10 July 2016

Academic Editor: Ilker S. Bayer

We demonstrate exceptional wetting-resistant surfaces capable of repelling low surface tension, non-Newtonian, and highly viscoelastic liquids. Theoretical analysis and experimental result confirm that a higher level of multiscale roughness topography composed of at least three structural length scales, ranging from nanometer to supermicron sizes, is crucial for the reduction of liquid-solid adhesion hysteresis. With Cassie-Baxter nonwetting state satisfied at all roughness length scales, the surface has been proven to effectively repel even highly adhesive liquid. Practically, this high-level hierarchical structure can be achieved through fractal-like structures of silica aggregates induced by siloxane oligomer interparticle bridges. The induced aggregation and surface functionalization of the silica particles can be performed simultaneously within a single reaction step, by utilizing trifunctional fluoroalkylsilane precursors that largely form a disordered fluoroalkylsiloxane grafting layer under the presence of sufficient native moisture preadsorbed at the silica surface. Spray-coating deposition of a particle surface layer on a precoated primer layer ensures facile processability and scalability of the fabrication method. The resulting low-surface-energy multiscale roughness exhibits outstanding liquid repellent properties, generating equivalent lotus effect for highly viscous and adhesive natural latex concentrate, with apparent contact angles greater than 160°, and very small roll-off angles of less than 3°.

1. Introduction

An advance in the field of liquid repellent surfaces has garnered much intention due to the underlying fundamentals and practical applications. Shortly after researchers gained an understanding of the key parameters behind the lotus effect phenomenon [1], a broad range of synthetic surfaces with extreme water resistance has experienced a surge of research publications [2–5] and impactful industrial exploitations [6–10]. These so-called superhydrophobic (water-repellent) surfaces generate apparent contact angles $\theta^* > 150^\circ$, together with small droplet roll-off angles typically $\alpha < 10^\circ$ for pure water [11]. Further, Tuteja et al. introduced effective design strategies dealing with low surface tension liquids [12] and demonstrated fabrications of superoleophobic (oil-repellent) surfaces, where an apparent contact angle greater than 150° as well as a very small roll-off angle ($\alpha < 10^\circ$) was also achieved for variety of organic solvents [13]. Recently, the combined effects of superhydrophobic and superoleophobic properties, namely, superomniphobic properties, have been introduced and acclaimed for their extraordinary liquid-repellent capabilities on virtually all liquids, both Newtonian and non-Newtonian [14]. These advancements in terms of liquid-repellent coating open many avenues for novel applications [15–18]. However, a majority of the studies so far has been confined within the regime of pure liquids [19–23] or dilute polymer solutions [14]. There are only a few articles discussing surfaces that can effectively repel complex fluids [24], especially those with viscoelastic behaviors, such as natural latex.

Natural rubber latex represents a class of complex liquid composed of ~35% of rubber microparticles dispersed in a water medium, where the water is later removed to achieve a high rubber concentration of ~60% when produced to an industrial standard [25]. Due to the high nonpolar polymer content, the latex liquid exhibits a fairly low surface tension

plus high adhesion and viscoelastic properties [26], such that the droplet can easily deform and spread on almost any surface that it comes into contact with. Moreover, natural rubber is among the most important industrial raw materials in the world, used for manufacturing many products, such as tires, gloves, conveyor belts, antivibration products, and so forth. The global production of natural rubber even at a farm level is valued at $25 billion a year with large production and consumption volumes of 12.11 and 12.13 million tons in 2014, respectively [27]. However, through the processes of harvesting, transporting, and manufacturing rubber latex, there is always liquid waste of about 10–15% due to adhesion [28]. Therefore, a latex-repellent coating would significantly help minimize the liquid loss and improve manufacturing efficiency.

The nature of low surface tension and high viscoelasticity, however, generally imposes unfavorable consequences on wetting behaviors: small contact angles and large rolling angle, respectively. In particular, viscoelasticity is known as the main origin of adhesion hysteresis where excessive energy is required to separate two attached surfaces [29]. This subsequently gives rise to the contact angle hysteresis phenomenon, where an advancing (wetting) contact angle is always greater than that of receding (dewetting) due to the increase of adhesive force at the peel-off liquid-solid contact line [30]. Larger contact angle hysteresis directly leads to increasing roll-off angles or oftentimes droplet pinning at the surface that diminishes the repellent ability even if a high contact angle is satisfied.

Low surface energy materials such as fluoroalkyl-functional compounds combined with a hierarchically rough topography containing reentrant curvatures have been proven in terms of their critical roles in supporting low surface tension liquids [12–14]. The available surface cavities at a micro-/nanoscale trap numerous air pockets underneath the liquid, which renders an effective surface heterogeneity composed of solid and air, resulting in a so-called Cassie-Baxter nonwetting state with an enlarged contact angle [31]. Meanwhile, droplet adhesion hysteresis is a strong function of the contact area between the liquid droplet and the solid surface. Thus, in order to achieve low adhesion hysteresis or a low resulting roll-off angle for viscoelastic droplets, it is important to minimize the actual wetted area by utilizing the surface-captured air pockets. Multiscale surface roughness, that is, surfaces with more than one length scale of roughness, that also satisfy a Cassie-Baxter condition should be an effective pathway to accomplish latex-repellent surfaces with an insignificant liquid-surface contact area, allowing droplets to roll easily.

Currently, most existing liquid-repellent surfaces make use of dual-scale surface roughness consisting of nanoscale features superposed on micron-sized textures [13, 14, 20–23]. In this research, however, we describe a facile fabrication method to produce higher-level multiscale roughness, at least up to four length scales. Inherently high fractal structures of silica aggregates are functionalized with fluoroalkylsilane functional groups under the presence of inherent moisture in order to achieve extended particle aggregation and growing fractal dimensionality, mediated by fluoroalkylsiloxane interparticle bridges [32]. The preexistence of absorbed water at silica surfaces has been reported to induce silane oligomeric grafting [33] and thus increases the achievable level of silane loading in the reaction [34]. With the fluoroalkyl moieties presumably projected outward, the resulting silica superstructures also possess low surface energy [35]. A simple and rapid coating process can be achieved through normal spray-on deposition over a precoated primer layer that addresses the scalability for large area coating. Finally, we also present a theoretical analysis of wetting properties on multiple-scale roughness, emphasizing the reduction of the actual wetted area fraction, which enhances apparent contact angles and reduces effective adhesion hysteresis that in turn allows for improved lower roll-off angles of the droplet even at high adhesion approximation.

2. Experimental

2.1. Materials. Precipitated silica particles (Ultrasil 7000 GR) were purchased from Evonik Industry. Acrylic resin powder (TKA-396) was supplied by Hangzhou Tiankai Enterprise. 2-Butoxyethanol (Butyl Cellosolve) was purchased from DOW Chemical Company. Fluoroalkylsilane coupling agents 1H,1H,2H,2H-perfluorodecyltriethoxysilane (FDTS), poly(vinylidene fluoride) (PVDF), toluene (AR grade), and acetone (AR grade) were obtained from Sigma-Aldrich. All chemicals and solvents were used as received. Preserved natural latex (*Hevea brasiliensis*) concentrate (industrial standard, 60% w/w of rubber in water medium) was obtained from Thai Rubber Latex.

2.2. Surface Functionalization and Induced Aggregation of Silica Particles. The method to fabricate a latex-repellent surface is schematically summarized in Figure 1**,** beginning with a surface chemical modification process. First, colloidal dispersion of precipitated silica particles was prepared by adding 0.5 g of silica into a flask containing 20 mL of toluene. Here, the native moisture of the original precipitated silica was determined to be $4.8 \pm 0.5\%$ w/w, while the water content in the toluene was trivial, $0.034 \pm 0.001\%$ w/w, measured by the Karl Fischer titration technique. The mixture of the silica and toluene was rigorously stirred for 30 min, followed by high-power ultrasonic homogenization for 15 min to ascertain highly homogeneous dispersion. Then, an appropriate amount of FDTS was slowly added into the flask, while stirring the suspension for uniform mixing. Maintained at ambient temperature, the functionalization reaction was allowed to proceed at a fixed stirring speed to ensure consistent shear rate and growth of silica particles upon siloxane-induced aggregation during the chemical surface functionalization. The result yielded a stock solution of low-surface-energy silica superstructures with increased fractal dimensionality. Here, the equimolar quantity of the FDTS grafting molecules and the silica surface silanol groups (Si-OH) was estimated from the specific BET surface area and the areal density of the available silanol sites on the silica surface. Typically, it has been reported that the maximum

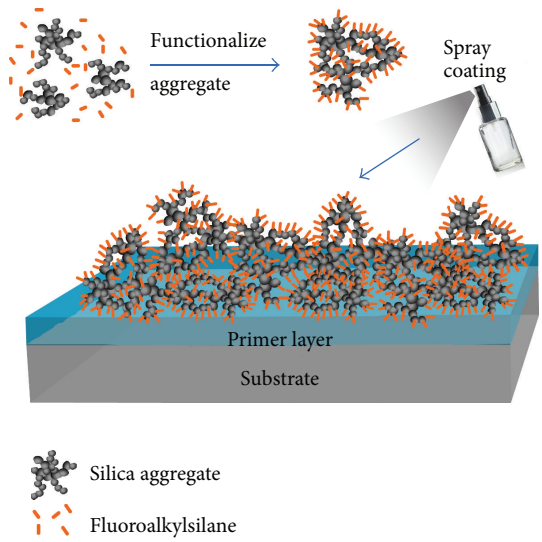

FIGURE 1: A brief procedure for the preparation of surface-modified silica aggregate coating solution and spray deposition on a substrate precoated with a primer layer.

surface density of reactive silanol for precipitated silica lies in the range of 4.6–4.9 silanols/nm^2 [36, 37]. However, the practically obtained grafting density of alkylsilane molecules has been reported for lower values: 2-3 molecules/nm^2 [38–40], which were estimated to 4 μmol/m^2. Therefore, with 0.5 g of precipitated silica, the required amount of the FDTS is 0.15 mL for 1 : 1 substitution. Furthermore, small variations of FDTS-silanol mole ratio (ϕ) were also studied; that is, $\phi = 1:3$, 2 : 3, 1 : 1, 4 : 3, and 5 : 3.

2.3. Preparation of Primer Solution. The primer solution for precoating was prepared from a polymer blend of PVDF and acrylic resin, furnishing with a good balance of adhesive and hydrophobic properties. PVDF powder, 1.25 g, was dissolved in a mixture of 20 mL toluene and 40 mL acetone and then agitated with a magnetic stirrer at a warm temperature of 45°C in a sealed container for 1 h. Afterwards, an equivalent amount of acrylic resin was added into the PVDF solution and stirred for another 5 h. Before use, 0.6 mL of high-boiling-point 2-butoxyethanol was added into the co-dissolved polymers to help slow down the evaporation rate at the eventual film drying, preventing possible film cracks due to capillary stress.

2.4. Spray Coating. Microscope glass slides with dimensions of 25 × 75 mm were used as substrates. Prior to the spray coating process, all substrates were cleaned through a RCA-1 cleaning protocol [41], followed by drying under N_2 stream. An adhesive primer layer was deposited by spray-coating the PVDF-Acrylic solution using a common disposable 20 mL glass bottle with a push spray head. For the coating on each sample, 10 mL of the primer solution was filled into the glass bottle, and the spray deposition was performed manually by pushing the spray head 10 times to achieve uniform surface coverage. Also, the distance between the substrate and the spray head was maintained at 10 cm, which is suitable for the mist to diffuse and cover the entire substrate. The primer layer was then left to dry at room temperature for 1 h. The top coat solution was formulated from a mixture of the stock solution, acetone and 2-butoxyethanol with a volume ratio of 1 : 2 : 0.03, and then deposited onto the dried primer layer with the same spray coating details. All samples were dried in ambient condition for at least 24 h before characterizations. To prevent a possible nonuniform mist profile emerging from a clogged spray head, a new piece of the spray equipment was used for every new substrate.

2.5. Characterizations. The wetting properties of coating surfaces were evaluated using three different types of liquid: distilled water, 35% w/w latex, and 60% w/w latex. Here, the 60% w/w latex concentrate was diluted with distilled water to achieve the 35% w/w latex, representing the average concentration of freshly tapped natural latex. The surface tensions of all liquids were determined by pendant drop technique [42], using the drop shape analysis feature in an optical contact angle measurement system (Dataphysics OCA-15EC). The same equipment was also employed to measure static contact angles and droplet roll-off angles. Contact angle measurement was performed using probe liquids of droplet size ~4 μL placed at multiple locations on a sample surface. For each measurement, a dispensed droplet was allowed settling time around 1 min to assure an equilibrium. The droplet roll-off angle measurement was carried out using an additional tilting stage with a droplet of size ~10 μL dispensed on a sample surface. The droplet was then set into motion by slowly adjusting the tilt angle. Multiple measurements were also investigated for tilt angles in both clockwise and counterclockwise directions. Primary silica particle size was determined by high-magnification transmission electron microscopy (TEM, JEOL JEM-2010), while the sizes of secondary, tertiary, and quaternary silica aggregates were investigated by laser diffraction particle size analyzers (Beckman Coulter LS 230). Surface topological structures of the coating film and particle aggregates were studied using scanning electron microscopy (SEM, FEI Quanta 400).

3. Results and Discussions

3.1. Surface Tension of Natural Latex. The surface tensions of water, 35% latex, and 60% latex were determined using a pendant drop technique performed at ambient temperature. The typical pendant drop shapes are displayed in Figure 2, and the corresponding calculation results of the surface tensions are shown in Table 1. The suspended drop volume and degree of shape deviation from a perfect sphere relate directly to the ratio between the weight of the drop and its surface tension. Roughly, the hanging drop volumes of latex liquids are comparatively smaller than the water, indicating lower surface tensions to hold the droplets against gravity.

With the density known, surface tension can be determined by geometrical analysis of the drop shapes. As shown in Table 1, it is clear that the surface tension of the liquid

Table 1: Density and surface tension of three different types of liquids: water, 35% latex, and 60% latex.

Liquids	Density (g/mL)	Surface tension (mN/m)
Water	0.99 ± 0.02	72.9 ± 0.2
35% latex	0.92 ± 0.04	44.2 ± 0.8
60% latex	0.87 ± 0.08	35.4 ± 0.7

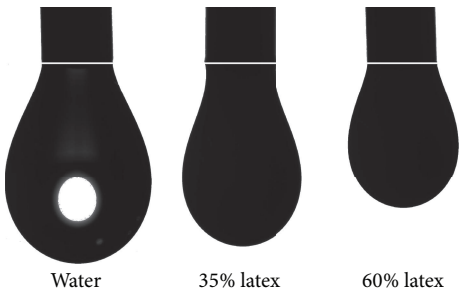

Figure 2: Photographs show pendant drops shapes of water, 30% latex, and 60% latex.

reduces as the percentage of rubber increases. This can be explained using a thermodynamic argument that the increasing amount of colloidal latex particles is favorable for adsorbing at the surface, reducing internal energy while increasing entropy of the dispersion, resulting in lower surface tension [43].

3.2. Wetting Properties of the Coating. Figure 3 displays the wetting properties of the spray-on coating surfaces, investigated by means of static contact angle measurement using sessile drops of water, 35% latex, and 60% latex. Interestingly, all water contact angles were significantly large, with $\theta^* > 150^\circ$ observed for all conditions, even for the samples intentionally prepared with a brief reaction time of ~15 min (data points presented at day 0). In general, silane grafting on silica surface at room temperature without an acid/base catalyst would require reaction times of tens of hours to several days in order to achieve maximum bonding density [44, 45]. In this case, the rapid particle functionalization can be attributed to the presence of water, especially the preadsorbed water on the silica surfaces that promotes the extents of hydrolysis and condensation reactions of the FDTS precursors. It is also indicative that the silane reaction can possibly continue more or less during the film drying stage [46].

Similar trends in contact angle responses were also observed for both 35% latex and 60% latex, except that the overall values of the contact angle decrease progressively for liquids with lower surface tension. Furthermore, all contact angle profiles exhibited plateaus starting at approximately day 3 of the reaction time, where contact angles greater than 150° prevailed for all types of the probed liquids. This reveals the predominance of the Cassie-Baxter nonwetting state and thus the effectiveness of the liquid-resistance capability. Maximum contact angles $\theta^*_{\max}$ ~175°, ~165°, and ~160° can be obtained for water, 35% latex, and 60% latex, respectively, which is beyond the standard requirement of 150°. Additionally, it was also observed that the variation in FDTS-silanol mole ratio, ϕ, poses an effect on the contact angle of all liquids, where higher values of ϕ generally impart a larger contact angle. In the case of $\phi < 1:1$, partial wetting, that is, Wenzel state, was noticed for latex liquids particularly at fewer days in reaction time.

Perhaps the best characterization to investigate the liquid-repellent ability of surfaces is done through droplet roll-off angle measurement, since large contact-angle surfaces do not always confirm liquid dynamics as a result of partial liquid impregnation that leads to high adhesion or droplet immobilization [47]. The results in Figure 4 display the roll-off angles characteristics of the same coating surfaces measured for water, 35% latex, and 60% latex, respectively. Again, there were excellent results for water, where a very low roll-off angle of $\alpha < 10^\circ$ was accomplished for all coating conditions. Combined with the aforementioned water contact angle properties, the superhydrophobic criteria were satisfied even within a short reaction time (~15 min) and at a low FDTS amount ($\phi = 1:3$). All liquids exhibit similar behaviors where their roll-off angles decrease with reaction time and also reach equilibrium values after ~3 days of the reaction. The minimum roll-off angle as low as $\alpha_{\min}$ ~1°, ~2°, and ~3° can be attained for water, 35% latex, and 60% latex, respectively, indicating extreme liquid repellency of the coating surfaces even for low surface tension and highly viscous latex concentrate. An example video of latex flow on a latex-repellent coated surface can be found in the Supplementary Material, available online at http://dx.doi.org/10.1155/2016/9510156. However, high roll-off angle cases were also observed for latex liquids with fewer FDTS content.

Deduced from the results above for both static contact angles and roll-off angles, relatively simple, monotonic qualitative relationships of the wetting performance versus surface tension, reaction time, and FDTS mole ratio can be established. As expected, the surfaces exhibit greater repellency for higher tension liquid like water, as the droplets tend to bead up and roll easily. However lower surface tension drop shapes are likely to deform, as illustrated in Figure 3 insets, lowering the contact angles, and hindering the droplet movements. Theoretical details concerning the effects of liquid surface tension will be discussed further in Section 3.4. The surface functionalization time and FDTS molar amount impose an effect on surface energy of the coating. Shorter reaction time and lower value of ϕ should lead to incomplete substitution of surface silanol groups by the fluoroalkylsilane moieties, resulting in inferior surface energy which is easily wetted by low surface tension liquids. On the contrary, for long duration time together with sufficient amount of FDTS molecules, excellent nonwetting properties can be attained for all liquids here. However, the effect of surface energy alone cannot produce such highly efficient liquid repellent properties. The discussion must involve the surface morphology effect of the deposited silica particles as described below.

3.3. Growth of Silica Aggregates and Surface Roughness. Multiscale roughness in micro and nano ranges is another key

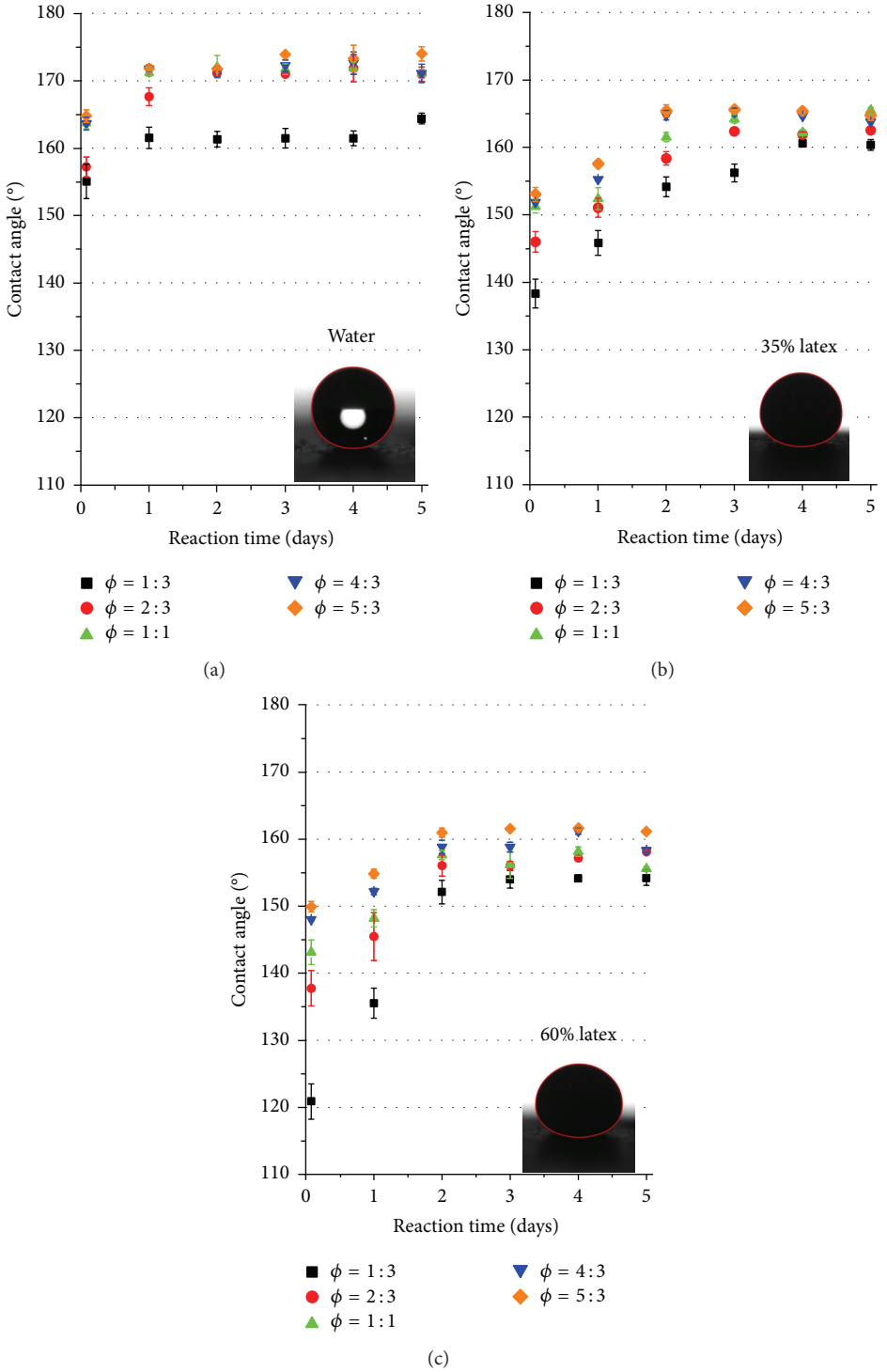

FIGURE 3: Contact angles measurements of (a) water, (b) 35% latex, and (c) 60% latex on flat samples coated with FDTS-modified silica for varied reaction time and FDTS-silanol mole ratio, ϕ. Each inset represents an example of droplet shape (with highlighted edge line) for ϕ = 1 : 1 at day 3 of reaction. Note that the data points located at day 0 actually represent a reaction time of 15 min.

component underlying the extreme nonwetting behaviors of the latex-repellent surfaces, which is obtained by uniform coverage of a silica nanoparticle layer. Here, the degree of hierarchical structures of the original precipitated silica can be further enhanced by siloxane-induced aggregation to form highly ramified superstructures. The fractal dimensionality of such complex particle structures extends with respect to the growing size of the silica aggregates, which happen simultaneously with the chemical functionalization reaction. Figure 5(a) shows the progressive extension of the aggregate size

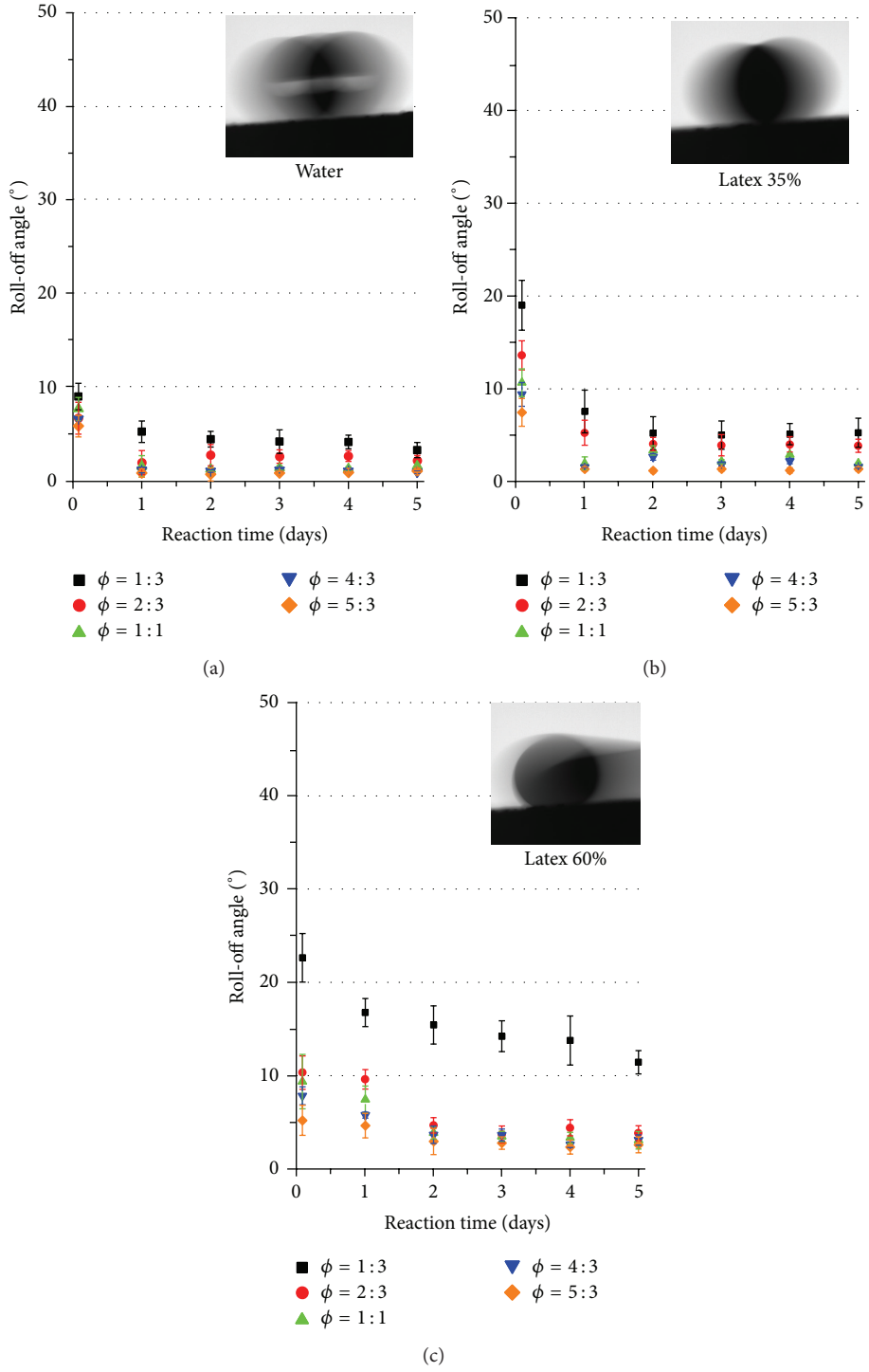

FIGURE 4: Droplet roll-off angle measurements of (a) water, (b) latex 35%, and (c) latex 60% on tilted substrates with precedent coatings of chemically surface-modified silica aggregates of varied functionalization time and FDTS-silanol mole ratio, ϕ. The insets show typical samples of droplet rolling on surface with $\phi = 1:1$, at day 3 of reaction, and with an inclined angle $\alpha \sim 5^{\circ}$.

over the reaction time, measured by laser diffraction particle size analyzers. It is worth noting that, for such nonspherical silica particles, the light diffraction technique provides an effective spherical radius of the aggregate structure. At the initial time (day 0), the most probable size of the aggregate, around 110 nm, is distinctively observed with a relatively narrow size distribution. This result agrees with the fact that the original precipitated silica does not normally exist as free primary particles (size ~ 15–20 nm), and rather more stable secondary aggregates will be formed by those primary particles fusing together [48]. Thus, the observable diffraction signal is mainly generated by the secondary particles or larger

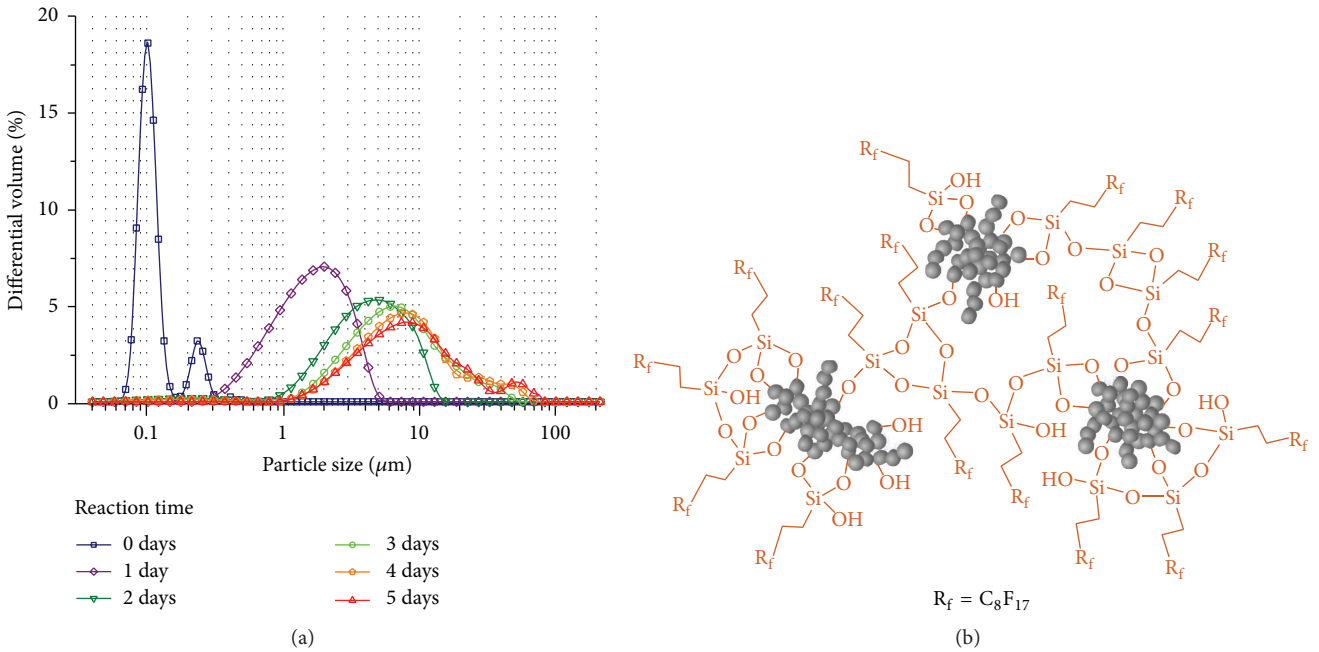

Figure 5: (a) Size evolution of silica aggregates throughout surface modification reaction measured by light diffraction technique. (b) The drawing (not to scale) of possible interparticle bridge triggered by siloxane oligomer, which mediates the particle aggregation.

clusters. There was also a small peak of larger particles sized at ~230 nm, indicating that the secondary particles started to combine with one another. The growth rate of the silica aggregates throughout the reaction was comparatively rapid at the beginning, that is, large fractions of the secondary particles combined into micron-sized particles almost within the first day of the reaction. Although silica aggregation in a colloidal dispersion is a diffusion-controlled process, the attachments between particles can be mediated by the short-range hydrogen bonds inherent to the surface silanol groups and the interlinkage formed by siloxane oligomer as illustrated in Figure 5(b). The FDTS molecules, possessing three hydrolysable groups, can undergo either direct surface grafting, or self-induced polycondensation in the presence of sufficient water, which forms a 3-D siloxane structure capable of connecting adjacent aggregates. The fluoroalkylsiloxane, to some extent, projects the disorder fluoroalkyl moieties toward the cluster surface. As such, the low surface energy requirement for the overall particle structure is still met. The growth rate tends to slow down and reaches equilibrium after approximately 3 days of the reaction, consistent with the plateau behavior of the surface wetting properties previously shown in Figures 3 and 4. At a late stage of the reaction, most of the surface silanol groups on the particles are replaced by the fluoroalkylsilanes and fluoroalkylsiloxanes, which passivate the surface from further attachments. Eventually, the tertiary and quaternary particles of large supermicron sizes are predominant with much broader size distribution ranging from ~1 μm to ~100 μm. This is approximately 2-3 orders of magnitude of increased size, in comparison with the size of the initial secondary particles at 110 nm.

Although the formation of a siloxane oligomer network can facilitate particle aggregation to achieve micron-scale roughness, it is necessary to ensure that the extent of the disordered silane and siloxane layers do not significantly compromise the nano-rough feature of the aggregate, inherently generated by the nano-sized primary particles. The silica aggregates were then examined at a high magnification using a TEM technique emphasized on the details of the primary particles, before and after the functionalization reaction. The TEM images are displayed in Figure 6, revealing that the size and shape of the primary silica particles were somewhat indistinguishable between the initial silica and those that had undergone the induced aggregation process for 3 days. This observation suggests that the moisture-induced fluoroalkylsilane oligomerizations pose virtually no effect on the ultrafine roughness feature at a nanometer length scale. More careful particle size measurements via TEM build-in imaging techniques, done with over 200 samplings of primary particles acquired from at least 50 individual aggregates, yielded average sizes of 15 ± 2 nm for the initial precipitated silica and 20 ± 4 nm for the silane-modified counterpart. The increase of the primary particle size upon surface functionalization was approximately 1.8 times the fully stretched FDTS fluoroalkyl chain length, indicating that the highly ordered 1 : 1 monolayer grafting on the silica surface was not a favorable process. Instead, this result supports the predominance of short siloxane grafting caused by the preadsorbed water at the silica surface. In principle, this oligomeric grafting should require a slightly larger amount of the FDTS, which can explain the improvement of the wetting properties at higher FDTS content; that is, $\phi > 1:1$.

To better describe the appearance of the fractal-like multiscale roughness obtained from the spray coating, a SEM technique was employed for detailed investigations of the surface topography. The images in Figure 7 show top-view

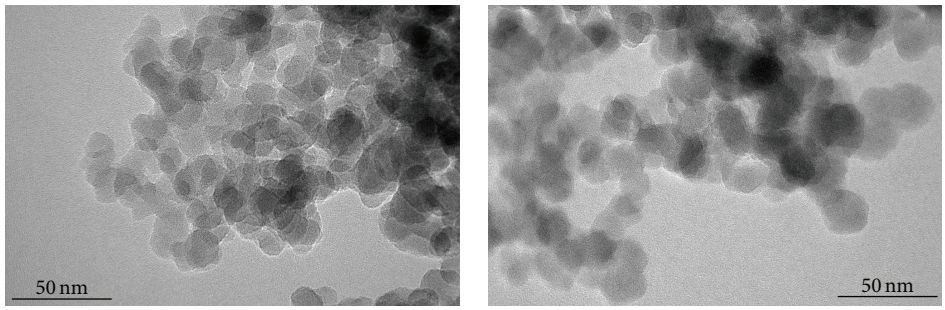

(a) (b)

Figure 6: TEM images of silica aggregates revealing size and shape of the primary particles for (a) initial precipitated silica and (b) after 3 days of fluoroalkylsilane surface modification.

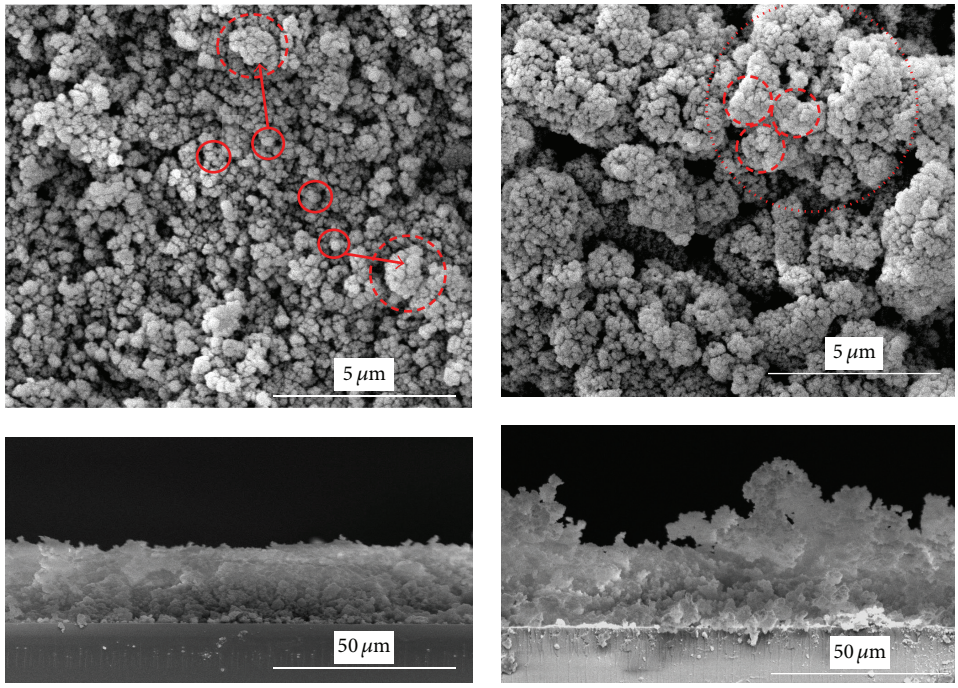

(a) (b)

Figure 7: SEM micrographs showing plane view (top) and cross section (bottom) of the nanoparticle coating films for (a) initial precipitated silica and (b) after 3 days of induced aggregation reaction. The solid and dashed circles indicate secondary and tertiary particles, respectively.

and cross-section surfaces of the coating layer comprising the functionalized silica aggregates. For the initial precipitated silica with minimal aggregation, shown in Figure 7(a), the surface roughness sizes around submicron scales, ~100–300 nm (corresponding to the secondary particles), were ubiquitous as marked by solid circles. This result is consistent with the initial particle size distribution revealed by the light diffraction technique. Larger aggregates (tertiary particles) up to ~1-2 microns were also observed as marked by the dashed circles, reflecting the compact combination of the secondary particles. The cross-sectional image displays a slow variation of surface topography at a larger tens of microns length scale. In contrast, higher-order hierarchical structures with multiple length scales of roughness size are commonly seen in Figure 7(b), taken from a coating after 3 days of induced aggregation. Supermicron-sized structures around ~5–50 μm (quaternary particles) are prevalent and composed mainly of tertiary aggregates, as indicated by the dotted circle. The self-similarity of these composite structures can be observed at quaternary, tertiary, and secondary levels confirming a high degree of fractal structures. The planar and cross-sectional images confirm the formation of reentrant curvatures at multiple length scales, generating surface cavities at a nano- and micro-range that are capable of trapping air pockets underneath a liquid. With the combination of such multiscale roughness and low surface energy imparted by fluoroalkylsilane, an effective Cassie-Baxter nonwetting state can be expected.

3.4. Theoretical Model of Wetting on Multiscale Roughness. To gain deeper insight regarding the unusual wetting properties imparted by multiscale roughness features of the silica superstructures, a theoretical model was developed based on the nonwetting Cassie-Baxter state. The below model does not intend to deliver accurate theoretical predictions for wetting behaviors of such stochastic topography; in fact, it may be impossible to do so. Rather, a less complicated yet more comprehensible mathematical model should be more useful for understanding the role of a complex morphology on effective liquid-repellent properties. Here, the surface roughness in several length scales was modeled by a fractal structure composed mainly of perfect spherical particles at different length scales, where larger spheres are uniformly covered by a layer of smaller spheres, as illustrated in Figure 8. The self-similarity of this structure is repeated throughout multiple length scales. The surface roughness can be characterized by sphere radii, R_i, and the distances from center to center of the spheres, L_i, where $i = 1, 2, 3 \ldots$ corresponds to the level of roughness from the smallest to a larger length scale. It is simply perceivable that the spherical particles at levels $i = 1$, 2, 3, and 4 are analogous to the primary, secondary, tertiary, and quaternary silica aggregates, respectively.

For any rough or heterogeneous surfaces, the general form of Cassie-Baxter nonwetting state reads [49]:

$$\cos\theta^* = rf_{\mathrm{SL}}\cos\theta_0 - f_{\mathrm{LA}}, \tag{1}$$

where $f_{\mathrm{SL}} + f_{\mathrm{LA}} = 1$ are, respectively, the solid-liquid and liquid-air flat area fractions of surface under liquid; r is the roughness factor defined as the ratio of a solid-liquid area to its projection on a plane; and θ_0 is Young's contact angle of an equivalent homogeneous smooth surface. Now consider roughness of one length scale, that is, a surface roughened by a single layer of identical spheres uniformly distributed across the surface as depicted in Figure 8 inset. Spherical particles of radius R_1 are separated by distance L_1 such that reentrant curvatures are formed with air pockets inside, preventing liquid from bulging in. The liquid penetration depth in the interparticle gap depends on the local equilibrium of interface energies: solid-air (γ_{SA}), solid-liquid (γ_{SL}) and liquid-air (γ_{LA}) which can be characterized by Young's contact angle θ_0 such that $\cos\theta_0 = (\gamma_{\mathrm{SA}} - \gamma_{\mathrm{SL}})/\gamma_{\mathrm{LA}}$. It is natural to assume that the spheres laterally distribute in the pattern of a hexagonal unit cell, so that the solid-liquid flat area fraction is $f_{\mathrm{SL}} = \Gamma_1 \sin^2\theta_0$. Here, $\Gamma_1 = (\pi/2\sqrt{3})(2R_1/L_1)^2$ is the dimensionless parameter related to the geometrical arrangement of the spherical particles on the surface area [50]. The roughness factor can be determined from the ratio of the wetted spherical cap to its projected circle as $r = 2(1 + \cos\theta_0)/\sin^2\theta_0$. Thus, the modified Cassie-Baxter equation for the first level of spherical roughness ($i = 1$) can be expressed as the following [50]:

$$\cos\theta_1^* = \Gamma_1\left(1 + \cos\theta_0\right)^2 - 1. \tag{2}$$

Equation (2) shows that the smooth-surface contact angle, θ_0, is amplified to the first-level apparent contact angle θ_1^* by the spherical roughness of one length scale, Γ_1.

The above theoretical prediction of wetting properties on single scale roughness can be further generalized for multilevel roughness. The wetting of a layer containing bigger spheres whose surfaces are roughened by smaller spheres should also be described by the above modified equation, except that the local contact angle θ_0 of the bigger spheres must be replaced by the apparent contact angle θ_1^* to account for the roughness effect from the smaller spheres. Therefore, the generalized form of the Cassie-Baxter nonwetting state at the ith level of spherical roughness can be expressed in the iteration form as

$$\cos\theta_i^* = \Gamma_i\left(1 + \cos\theta_{i-1}^*\right)^2 - 1. \tag{3}$$

Here, $\Gamma_i = (\pi/2\sqrt{3})(2R_i/L_i)^2$ becomes the geometric parameter associated with the roughness at the ith level. The above equation suggests $\theta_i^* > \theta_{i-1}^*$; that is, the apparent contact angle becomes larger for higher-level surface roughness, and hence liquid penetration becomes more difficult at larger scales. Equation (3) assumes the same surface chemical composition for all spheres, as well as satisfaction of the Cassie-Baxter state at all length scales. Note that the latter assumption is accurate only for the first few values of i where the gap dimension does not exceed liquid capillary length, $\ell = (\gamma_{\mathrm{LA}}/\rho g)^{1/2}$; otherwise, the weight effect will cause liquid to sag in and wet the gaps, giving rise to a more complicated wetting situation. In fact, $\ell \sim 650\,\mu$m was obtained for a latex concentrate, indicating that the full Cassie-Baxter approximation was still accurate at least up to $i = 5$.

The calculation for contact angles based on the above theoretical model was performed using input parameters of Young contact angles as $\theta_0 = 109.2$, 93.1, and 83.2 for water, 30% liquid, and 60% latex, respectively. They were obtained from contact angles measurements on smooth glass (SiO_2) substrates, coated with FDTS molecules. The geometric ratio $2R_i/L_i = 0.8$ was assumed for all length scales to account for the compact aggregate structures. Figure 9 shows the resulting calculations of apparent contact angles of liquids sitting on multiscale roughness composed of up to 4 different length scales; for example, $i = 1$, 2, 3, and 4. It is clear that the apparent contact angles of all liquids increase considerably with higher levels of roughness structures, and the values approach 180° even for the low surface tension latex concentrate. This ascertains the critical role of such multiscale roughness on the outstanding liquid-shielding behaviors. It is helpful noting that the above predicted contact angles for $i = 2$–4 are comparable to the experimental results from days 0–3 shown in Figure 3, where the real roughness structures start growing from secondary particles to eventually become quaternary particles. For water, the calculated contact angles above 150° were already obtained for $i \geq 2$, which is in good agreement with the experimental contact angles at day 0 where secondary silica particles were predominant on the coating surface. However, more roughness length scales, such as $i \geq 3$, are required in order for latex liquids to achieve $\theta^* > 150°$. This explains the need of longer reaction time for the practical latex-repellent coatings.

In terms of roll-off angle characteristics, the physical reasons underlying the existence of an angle threshold for dynamic wetting are still not fully understood. However, it is believed that several parameters such as adhesion hysteresis,

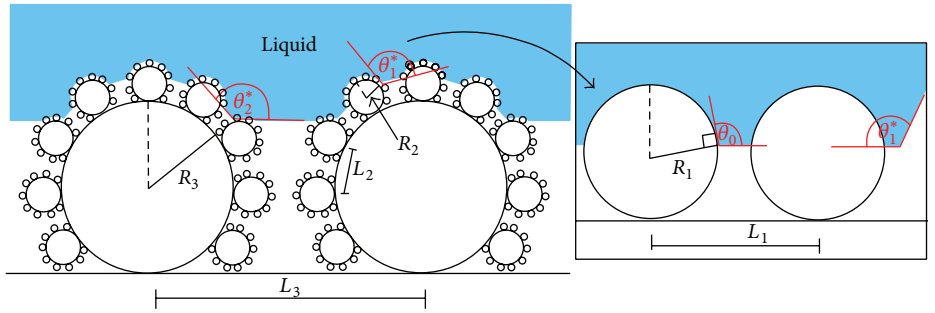

FIGURE 8: Schematic representation of Cassie-Baxter State on multiscale roughness, modeled by sphere-based fractal. Roughness parameters such as R_i and L_i represent the radius and interparticle distance for a roughness at ith level.

surface roughness, and heterogeneity are the principal factors determining the size of the roll-off angles. Recently, previous works have demonstrated that the dynamic wetting properties such as droplet adhesion and contact angle hysteresis can be either increased or reduced in a controllable manner, by properly configuring surface structure into multiple scale roughness [51, 52]. These findings firmly indicate the significant role of complex surface roughness upon dynamic wetting properties. The following model also exploits the effect of multiple length scale roughness to counteract with highly adhesive droplet. Here, the roll-off contact angle α for a droplet with mass m can be estimated by making use of an energy balance method as [30]

$$\sin\alpha = \frac{\Delta W_0 l\,(rf_{SL})}{mg}, \tag{4}$$

where ΔW_0 is the adhesion hysteresis (work per unit area) of liquid on a smooth surface and l is the length of a liquid-solid contact line associated with the circular contact area of $(1/4)\pi l^2$. Essentially, the adhesion hysteresis is a complex phenomenon, suggesting that the energy required to separate two attached bodies is always greater than the energy of bringing them into contact. The ΔW_0 could originate from several energy-dissipating sources, especially viscoelastic effects at both macroscopic and microscopic scales [53, 54].

The droplet-surface contact line l, for such extreme nonwetting surface, depends mainly on the effect of gravity that deviates the droplet shape from a perfect sphere, as illustrated in Figure 10. Given a droplet of radius R_d, density ρ, and surface tension γ_{LA}, the order of l can be estimated by the scaling law below [55]:

$$l \sim \left(\frac{\rho g}{\gamma_{LA}}\right)^{1/2} R_d^2, \tag{5}$$

which suggests that low surface tension liquids, for example, latex, should have greater shape deformation when compared to water. This argument is congruous with the real drop shapes shown in Figure 3 insets. Generally, a longer l leads to a larger liquid touching area where more energy can dissipate due to viscoelastic contact and hence intensifies the roll-off angle.

The effect of the roughness factor rf_{SL} on the roll-off angle is even more profound than other parameters as it determines

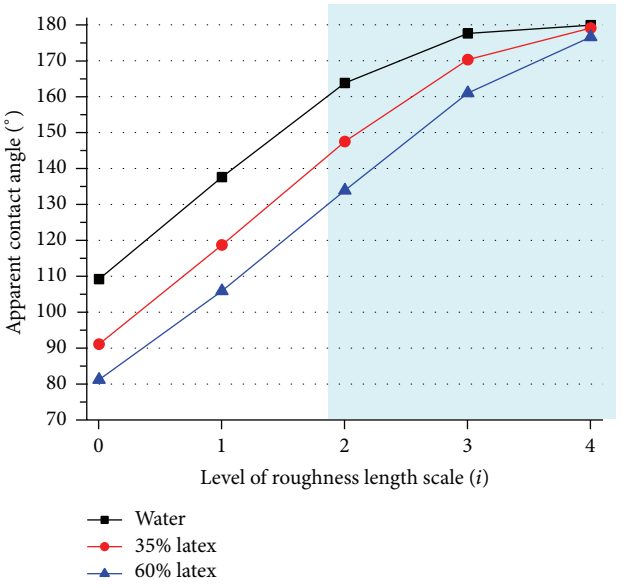

FIGURE 9: Theoretical approximation of apparent contact angles for water, 35% latex, and 60% latex liquids, sitting on surface roughness of multiple length scales.

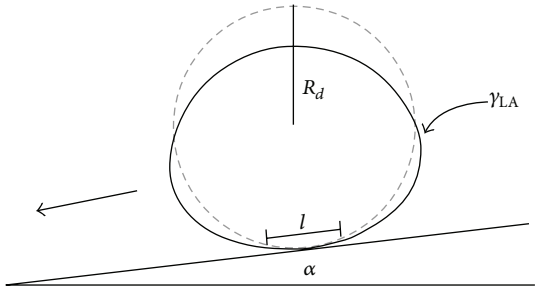

FIGURE 10: Schematic representation of droplet shape deformation when subjected to gravity.

the actual liquid-solid contact area. The above model of spherical roughness shows that the area fraction of liquid that actually wets the solid surface becomes much less with increasing levels of roughness. Thus, it is quite rational that the effective wetted area fraction can be estimated from the

product of rf_{SL} for all length scales constituent the roughness, such that

$$(rf_{SL})_i = \prod_{n=1}^{i} (rf_{SL})_n = \prod_{n=1}^{i} \Gamma_n \left(1 + \cos\theta^*_{n-1}\right). \quad (6)$$

Since normally the roughness factor $rf_{SL} < 1$ applies for all scales, the product of (6) should rapidly decrease upon the addition of roughness length scale, implying that the effective liquid-solid contacted area is greatly reduced through the multiple scale roughness. To further visualize the effect of the roughness on roll-off angle, (4) is plotted using the effective rf_{SL} evaluated in (6). To simplify the calculation, it is assumed that the order of adhesion hysteresis is comparable to gravitational potential energy as follows:

$$\frac{\Delta W_0 l}{mg} \sim 1. \quad (7)$$

The above approximation lies in a fairly high adhesion regime, which suites the latex droplets. The roll-off angles for water, 30% latex, and 60% latex liquids versus the level of surface roughness length scale are calculated as displayed in Figure 11.

The theoretical model reveals a common trend where the roll-off angles for all liquids fall rapidly with regard to the increment of roughness length scales. The calculation points at $i = 0$ cannot be made, reflecting the fact that all liquids here wet the smooth surface fairly well; therefore the droplets are likely to pin on the surface. Again, the calculation results for $i = 2$–4 match with the measured roll-off angle results of days 0–3 displayed in Figure 4. The calculations show that a rough surface can generate superhydrophobic properties with $\alpha < 10^\circ$ for $i \geq 2$, while $i \geq 3$ is required for latex liquids to achieve similarly small values of roll-off angles. The results point out that the design of a latex-repellent coating requires surface roughness comprised of at least three levels of roughness length scales. Furthermore, very low roll-off angles approaching 0° can be attained for roughness consisting of four length scales even when a high adhesion approximation is made. This can explain the extremely small roll-off angles of ~1°, ~2°, and ~3° experimentally obtained for water, 30% latex, and 60% latex, respectively. These properties exist even for highly adhesive, viscoelastic latex liquids as the liquid does not significantly touch the surface.

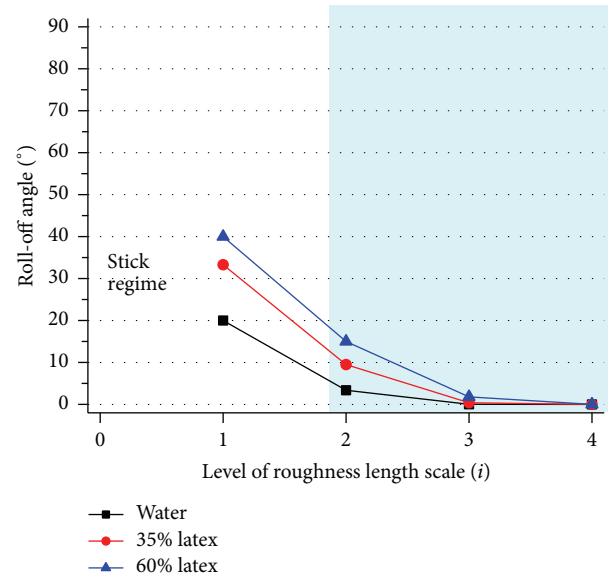

Figure 11: Theoretical approximation of roll-off angles for water, 35% latex, and 60% latex liquids rolling on surface roughness of multiple length scales. There is no roll-off angle for a smooth surface, $i = 0$.

4. Conclusion

This work presented a facile coating formulation containing fractal-like silica superstructures formed by siloxane oligomer interparticle connection, taking place simultaneously with the silica surface functionalization reaction. The employed fluoroalkylsilane precursors, containing three-hydrolysable groups, tended to generate disordered fluoroalkylsiloxane grafting in the presence of silica native moisture. This process facilitates silica aggregation and further extends their hierarchical structures, ranging from tens of nanometers to supermicron length scales. This coating has been demonstrated to be a useful class of liquid resistance materials capable of repelling even highly concentrated, viscoelastic latex liquids with low surface tension. Multiscale roughness topography composed of at least three length scales was experimentally and theoretically proven to be at the heart of the exceptional latex-repellent behaviors. With low surface energy imparted from the fluoroalkyl moieties, a Cassie-Baxter nonwetting state was assumedly satisfied at all roughness length scales, which significantly decreases the actual liquid-solid contact area and thus greatly reduces the effective adhesion hysteresis and hence roll-off angles. The resulting apparent contact angles were greater than 160°, with very small roll-off angles of less than 3° that can be accomplished for highly adhesive latex liquids.

Competing Interests

The authors declare that there is no conflict of interests regarding the publication of this paper.

Acknowledgments

This work was financially supported by the Thailand Research Fund (TRF) and Prince of Songkla University (Contract no. TRG 5880145), as well as the Center of Excellence in Nanotechnology for Energy (CENE), Prince of Songkla University.

References

[1] W. Barthlott and C. Neinhuis, "Purity of the sacred lotus, or escape from contamination in biological surfaces," *Planta*, vol. 202, no. 1, pp. 1–8, 1997.

[2] L. Gao and T. J. McCarthy, "How Wenzel and Cassie were wrong," *Langmuir*, vol. 23, no. 7, pp. 3762–3765, 2007.

[3] V. A. Ganesh, H. K. Raut, A. S. Nair, and S. Ramakrishna, "A review on self-cleaning coatings," *Journal of Materials Chemistry*, vol. 21, no. 41, pp. 16304–16322, 2011.

[4] X. Zhang, L. Wang, and E. Levänen, "Superhydrophobic surfaces for the reduction of bacterial adhesion," *RSC Advances*, vol. 3, no. 30, pp. 12003–12020, 2013.

[5] S. Nagappan and C.-S. Ha, "Emerging trends in superhydrophobic surface based magnetic materials: fabrications and their potential applications," *Journal of Materials Chemistry A*, vol. 3, no. 7, pp. 3224–3251, 2015.

[6] L. Cao, A. K. Jones, V. K. Sikka, J. Wu, and D. Gao, "Anti-Icing superhydrophobic coatings," *Langmuir*, vol. 25, no. 21, pp. 12444–12448, 2009.

[7] M. Shateri Khalil-Abad and M. E. Yazdanshenas, "Superhydrophobic antibacterial cotton textiles," *Journal of Colloid and Interface Science*, vol. 351, no. 1, pp. 293–298, 2010.

[8] H. J. Gwon, Y. Park, C. W. Moon et al., "Superhydrophobic and antireflective nanograss-coated glass for high performance solar cells," *Nano Research*, vol. 7, no. 5, pp. 670–678, 2014.

[9] Y. Wei, L. Hongtao, and Z. Wei, "Preparation of anti-corrosion superhydrophobic coatings by an Fe-based micro/nano composite electro-brush plating and blackening process," *RSC Advances*, vol. 5, no. 125, pp. 103000–103012, 2015.

[10] C.-H. Xue, X.-J. Guo, J.-Z. Ma, and S.-T. Jia, "Fabrication of robust and antifouling superhydrophobic surfaces via surface-initiated atom transfer radical polymerization," *ACS Applied Materials and Interfaces*, vol. 7, no. 15, pp. 8251–8259, 2015.

[11] B. Bushnan, *Springer Handbook of Nanotechnology*, Edited by B. Bushnan, Springer, New York, NY, USA, 3rd edition, 2010.

[12] A. Tuteja, W. Choi, M. Ma et al., "Designing superoleophobic surfaces," *Science*, vol. 318, no. 5856, pp. 1618–1622, 2007.

[13] A. K. Kota, Y. Li, J. M. Mabry, and A. Tuteja, "Hierarchically structured superoleophobic surfaces with ultralow contact angle hysteresis," *Advanced Materials*, vol. 24, no. 43, pp. 5838–5843, 2012.

[14] S. Pan, A. K. Kota, J. M. Mabry, and A. Tuteja, "Superomniphobic surfaces for effective chemical shielding," *Journal of the American Chemical Society*, vol. 135, no. 2, pp. 578–581, 2013.

[15] P. S. Brown and B. Bhushan, "Mechanically durable, superoleophobic coatings prepared by layer-by-layer technique for anti-smudge and oil-water separation," *Scientific Reports*, vol. 5, article 8701, 2015.

[16] L. Feng, Z. Zhang, Z. Mai et al., "A super-hydrophobic and super-oleophilic coating mesh film for the separation of oil and water," *Angewandte Chemie—International Edition*, vol. 43, no. 15, pp. 2012–2014, 2004.

[17] L. Li, H. Pan, J. Tao et al., "Repair of enamel by using hydroxyapatite nanoparticles as the building blocks," *Journal of Materials Chemistry*, vol. 18, no. 34, pp. 4079–4084, 2008.

[18] B. Bhushan, "Biomimetics inspired surfaces for drag reduction and oleophobicity/philicity," *Beilstein Journal of Nanotechnology*, vol. 2, no. 1, pp. 66–84, 2011.

[19] E. Bormashenko, R. Grynyov, G. Chaniel, H. Taitelbaum, and Y. Bormashenko, "Robust technique allowing manufacturing superoleophobic surfaces," *Applied Surface Science*, vol. 270, pp. 98–103, 2013.

[20] H.-B. Jo, J. Choi, K.-J. Byeon, H.-J. Choi, and H. Lee, "Superhydrophobic and superoleophobic surfaces using ZnO nano-in-micro hierarchical structures," *Microelectronic Engineering*, vol. 116, pp. 51–57, 2014.

[21] K. Nakayama, E. Tsuji, Y. Aoki, and H. Habazaki, "Fabrication of superoleophobic hierarchical surfaces for low-surface-tension liquids," *RSC Advances*, vol. 4, no. 58, pp. 30927–30933, 2014.

[22] W. Kwak and W. Hwang, "Facile method for preparing superoleophobic surfaces with hierarchical microcubic/nanowire structures," *Nanotechnology*, vol. 27, no. 5, Article ID 055301, 2015.

[23] T. P. N. Nguyen, R. Boukherroub, V. Thomy, and Y. Coffinier, "Micro-and nanostructured silicon-based superomniphobic surfaces," *Journal of Colloid and Interface Science*, vol. 416, pp. 280–288, 2014.

[24] A. Milionis, K. Dang, M. Prato, E. Loth, and I. S. Bayer, "Liquid repellent nanocomposites obtained from one-step water-based spray," *Journal of Materials Chemistry A*, vol. 3, no. 24, pp. 12880–12889, 2015.

[25] I. Franta, Ed., *Elastomers and Rubber Compounding Materials*, Elsevier Science, New York, NY, USA, 1st edition, 1989.

[26] G. Bauer, C. Friedrich, C. Gillig, F. Vollrath, T. Speck, and C. Holland, "Investigating the rheological properties of native plant latex," *Journal of the Royal Society Interface*, vol. 11, no. 90, Article ID 20130847, 2014.

[27] I. R. S. Group, *Rubber Statistical Bulletin*, International Rubber Study Group, 2015.

[28] G. Mathew, R. P. Singh, N. R. Nair, and S. Thomas, "Recycling of natural rubber latex waste and its interaction in epoxidised natural rubber," *Polymer*, vol. 42, no. 5, pp. 2137–2165, 2001.

[29] C.-Y. Hui, J. M. Baney, and E. J. Kramer, "Contact mechanics and adhesion of viscoelastic spheres," *Langmuir*, vol. 14, no. 22, pp. 6570–6578, 1998.

[30] B. Bhushan, M. Nosonovsky, and C. J. Yong, "Towards optimization of patterned superhydrophobic surfaces," *Journal of the Royal Society Interface*, vol. 4, no. 15, pp. 643–648, 2007.

[31] A. B. D. Cassie and S. Baxter, "Wettability of porous surfaces," *Transactions of the Faraday Society*, vol. 40, pp. 546–551, 1944.

[32] N. García, E. Benito, P. Tiemblo, M. M. B. Hasan, A. Synytska, and M. Stamm, "Chemically guided topography in alkylsilane- and oligosiloxane-modified silica nanoparticle coatings: from very hydrophobic surfaces to 'pearl' bouncing droplets," *Soft Matter*, vol. 6, no. 19, pp. 4768–4776, 2010.

[33] S. Brandriss and S. Margel, "Synthesis and characterization of self-assembled hydrophobic monolayer coatings on silica colloids," *Langmuir*, vol. 9, no. 5, pp. 1232–1240, 1993.

[34] R. E. Majors and M. J. Hopper, "Studies of siloxane phases bonded to silica gel for use in high performance liquid chromatography," *Journal of Chromatographic Science*, vol. 12, no. 12, pp. 767–778, 1974.

[35] A. Y. Fadeev and T. J. McCarthy, "Self-assembly is not the only reaction possible between alkyltrichlorosilanes and surfaces: monomolecular and oligomeric covalently attached layers of dichloro- and trichloroalkylsilanes on silicon," *Langmuir*, vol. 16, no. 18, pp. 7268–7274, 2000.

[36] L. T. Zhuravlev and V. V. Potapov, "Density of silanol groups on the surface of silica precipitated from a hydrothermal solution," *Russian Journal of Physical Chemistry A*, vol. 80, no. 7, pp. 1119–1128, 2006.

[37] Q. Wan, C. Ramsey, and G. Baran, "Thermal pretreatment of silica composite filler materials," *Journal of Thermal Analysis and Calorimetry*, vol. 99, no. 1, pp. 237–243, 2010.

[38] L. Boksányi, O. Liardon, and E. S. Kováts, "Chemically modified silicon dioxide surfaces Reaction of *n*-alkyldimethylsilanols and *n*-oxaalkyldimethylsilanols with the hydrated surface of silicon

dioxide—the question of the limiting surface concentration," *Advances in Colloid and Interface Science*, vol. 6, no. 2, pp. 95–137, 1976.

[39] D. W. Sindorf and G. E. Maciel, "Cross-polarization/magic-angle-spinning silicon-29 nuclear magnetic resonance study of silica gel using trimethylsilane bonding as a probe of surface geometry and reactivity," *The Journal of Physical Chemistry*, vol. 86, no. 26, pp. 5208–5219, 1982.

[40] F. Bernardoni, M. Kouba, and A. Y. Fadeev, "Effect of curvature on the packing and ordering of organosilane monolayers supported on solids," *Chemistry of Materials*, vol. 20, no. 2, pp. 382–387, 2008.

[41] W. Kern, *Handbook of Semiconductor Wafer Cleaning Technology: Science Technology, and Applications*, Edited by W. Kern, Noyes Publications, Park Ridge, NJ, USA, 1993.

[42] C. E. Stauffer, "The measurement of surface tension by the pendant drop technique," *The Journal of Physical Chemistry*, vol. 69, no. 6, pp. 1933–1938, 1965.

[43] L. Dong and D. Johnson, "Surface tension of charge-stabilized colloidal suspensions at the water-air interface," *Langmuir*, vol. 19, no. 24, pp. 10205–10209, 2003.

[44] E. Péré, H. Cardy, V. Latour, and S. Lacombe, "Low-temperature reaction of trialkoxysilanes on silica gel: a mild and controlled method for modifying silica surfaces," *Journal of Colloid and Interface Science*, vol. 281, no. 2, pp. 410–416, 2005.

[45] S. Gauthier, J. P. Aimé, T. Bouhacina, A. J. Attias, and B. Desbat, "Study of grafted silane molecules on silica surface with an atomic force microscope," *Langmuir*, vol. 12, no. 21, pp. 5126–5137, 1996.

[46] Y. Yang, A. M. Bittner, S. Baldelli, and K. Kern, "Study of self-assembled triethoxysilane thin films made by casting neat reagents in ambient atmosphere," *Thin Solid Films*, vol. 516, no. 12, pp. 3948–3956, 2008.

[47] B. Bhushan and E. K. Her, "Fabrication of superhydrophobic surfaces with high and low adhesion inspired from rose petal," *Langmuir*, vol. 26, no. 11, pp. 8207–8217, 2010.

[48] U. Kätzel, M. Vorbau, M. Stintz, T. Gottschalk-Gaudig, and H. Barthel, "Dynamic light scattering for the characterization of polydisperse fractal systems: II. Relation between structure and DLS results," *Particle and Particle Systems Characterization*, vol. 25, no. 1, pp. 19–30, 2008.

[49] Y. C. Jung and B. Bhushan, "Contact angle, adhesion and friction properties of micro-and nanopatterned polymers for superhydrophobicity," *Nanotechnology*, vol. 17, no. 19, article no. 033, pp. 4970–4980, 2006.

[50] S. S. Chhatre, W. Choi, A. Tuteja et al., "Scale dependence of omniphobic mesh surfaces," *Langmuir*, vol. 26, no. 6, pp. 4027–4035, 2010.

[51] A. T. Paxson and K. K. Varanasi, "Self-similarity of contact line depinning from textured surfaces," *Nature Communications*, vol. 4, article 1492, 2013.

[52] A. Milionis, D. Fragouli, L. Martiradonna et al., "Spatially controlled surface energy traps on superhydrophobic surfaces," *ACS Applied Materials & Interfaces*, vol. 6, no. 2, pp. 1036–1043, 2014.

[53] P. Attard, "Interaction and deformation of elastic bodies: origin of adhesion hysteresis," *The Journal of Physical Chemistry B*, vol. 104, no. 45, pp. 10635–10641, 2000.

[54] J. N. Israelachvili, "Adhesion, friction and lubrication of molecularly smooth surfaces," in *Fundamentals of Friction: Macroscopic and Microscopic Processes*, vol. 220 of *NATO ASI Series: E: Applied Sciences*, pp. 351–385, Springer, Dordrecht, The Netherlands, 1992.

[55] L. Mahadevan and Y. Pomeau, "Rolling droplets," *Physics of Fluids*, vol. 11, no. 9, pp. 2449–2453, 1999.